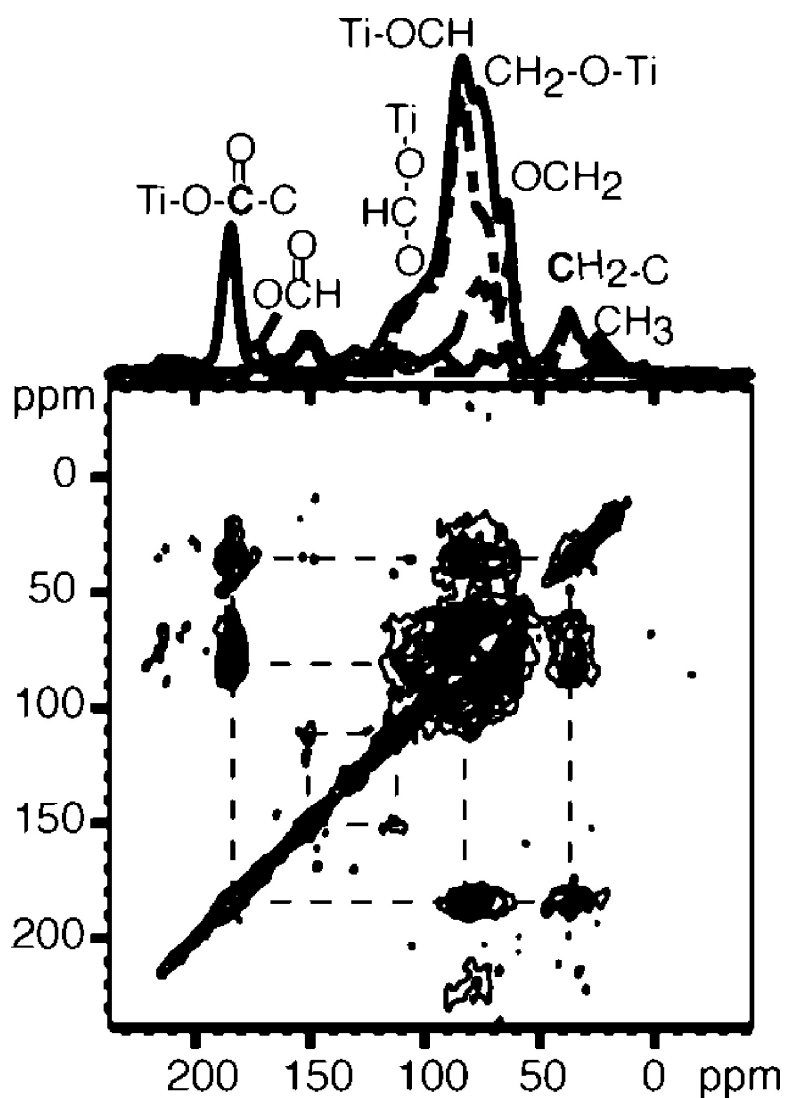


## Solid-State C NMR Characterization of Carbon-Modified TiO

Erin M. Rockafellow, Xiaowen Fang, Brian G. Trewyn, Klaus Schmidt-Rohr, and William S. Jenks

*Chem. Mater.*, Article ASAP • DOI: 10.1021/cm8019445 • Publication Date (Web): 16 March 2009

Downloaded from <http://pubs.acs.org> on March 24, 2009



# CHEMISTRY OF MATERIALS

Subscriber access provided by Iowa State University | Library

## More About This Article

---

Additional resources and features associated with this article are available within the HTML version:

- Supporting Information
- Access to high resolution figures
- Links to articles and content related to this article
- Copyright permission to reproduce figures and/or text from this article

[View the Full Text HTML](#)

# Solid-State $^{13}\text{C}$ NMR Characterization of Carbon-Modified $\text{TiO}_2$

Erin M. Rockafellow, Xiaowen Fang, Brian G. Trewyn, Klaus Schmidt-Rohr,\* and William S. Jenks\*

Department of Chemistry, Iowa State University, Ames, Iowa 50011-3111

Received July 16, 2008. Revised Manuscript Received January 29, 2009

$^{13}\text{C}$ -modified  $\text{TiO}_2$  was prepared to facilitate study of the dopant atoms and trace their chemical fate throughout the process. In the preannealed material, NMR showed strong evidence of many Ti–O–C bonds. After annealing, surface-bound coke is a major component. NMR also showed that a washing step before annealing led to the generation of orthocarbonate ( $\text{C}(\text{OR})_4$ ) centers, observed at 126 ppm, which are located deep inside the  $\text{TiO}_2$  particles. Both NMR and XPS confirmed the presence of small amounts of regular  $\text{sp}^2$ -hybridized carbonate species in all briefly annealed samples, while annealing for longer times led to a reduction removal of the  $\text{CO}_n$  centers. Quantitative NMR also shows the degree of carbon loss that accompanies annealing. Some variation in the chemical degradation of quinoline is noted among the catalysts, but coke-containing  $\text{TiO}_2$  catalysts are not qualitatively better catalysts for use with visible light with this substrate.

## Introduction

It is well-known that titanium dioxide is one of the most effective photocatalysts for the complete mineralization of pollutants in water and air.<sup>1–8</sup> However, although  $\text{TiO}_2$  is cheap, robust, and thermally stable, it is not yet ideal.<sup>9,10</sup> The two most important shortcomings are a low efficiency of photon usage due to rapid recombination of separated charges and that the onset of absorption, near 400 nm, does not allow sufficient use of terrestrial solar light.

Doping the  $\text{TiO}_2$ , either with main group elements or transition metals, has emerged as a promising approach for improving the catalyst.<sup>8,10,11</sup> Transition metal dopants have been shown to increase visible absorbance, but the experimental observations often include a decrease in the overall efficiency of the photocatalyst and sometimes thermal instability.<sup>12–16</sup>

Nitrogen-,<sup>17–21</sup> sulfur-,<sup>22–25</sup> and carbon-doped<sup>24,26–33</sup> titanium dioxides have displayed efficient photocatalytic degradation of some small organic molecules and dyes under visible irradiation. In these materials, the recombination center problem is minimized, if not eliminated.<sup>34–37</sup> Main group doping increases visible absorption by creating narrow, localized bands of orbitals within the band gap, as well as by promoting other defects of the  $\text{TiO}_2$  lattice.<sup>38–45</sup> For example, nitrogen doping of  $\text{TiO}_2$  has been correlated to an increase in oxygen vacancies, which are

\* Corresponding authors. E-mail: srohr@iastate.edu (K.S.-R.), wsjenks@iastate.edu (W.S.J.).

- (1) *Photocatalysis: Fundamentals and Applications*; Serpone, N., Pelizzetti, E., Eds.; John Wiley & Sons: New York, 1989.
- (2) Pichat, P.; Guillard, C.; Maillard, C.; Amalric, L.; D'Oliveira, J. C. *Trace Met. Environ.* **1993**, *3*, 207–223 (Photocatalytic Purification and Treatment of Water and Air).
- (3) Mills, A.; Davies, R. H.; Worsley, D. *Chem. Rev.* **1993**, *22*, 417–425.
- (4) Malati, M. A. *Environ. Technol.* **1995**, *16*, 1093–1099.
- (5) Bahnemann, D.; Cunningham, J.; Fox, M. A.; Pelizzetti, E.; Pichat, P.; Serpone, N. In *Aquatic and Surface Photochemistry*; Helz, G. R., Zepp, R. G., Crosby, D. G., Eds.; Lewis Publishers: Boca Raton, 1994, pp 261–316.
- (6) Serpone, N.; Khairutdinov, R. F. *Stud. Surf. Sci. Catal.* **1997**, *103*, 417–444.
- (7) Konstantinou, I. K.; Albanis, T. A. *Appl. Catal., B* **2003**, *42*, 319–335.
- (8) Fox, M. A.; Dulay, M. T. *Chem. Rev.* **1993**, *93*, 341–357.
- (9) Legrini, O.; Oliveros, E.; Braun, A. M. *Chem. Rev.* **1993**, *93*, 671–698.
- (10) Linsebigler, A. L.; Lu, G.; Yates, J. T., Jr. *Chem. Rev.* **1995**, *95*, 735–758.
- (11) Thompson, T. L.; Yates, J. T., Jr. *Chem. Rev.* **2006**, *106*, 4428–4453.
- (12) Choi, W.; Termin, A.; Hoffmann, M. R. *J. Phys. Chem.* **1994**, *98*, 13669–13679.
- (13) Anpo, M. *Catal. Surv. Jpn.* **1997**, *1*, 169–179.

- (14) Wang, C.-Y.; Bahnemann, D. W.; Dohrmann, J. K. *Chem. Commun.* **2000**, 1539–1540.
- (15) Coloma, F.; Marquez, F.; Rochester, C. H.; Anderson, J. A. *Phys. Chem. Chem. Phys.* **2000**, *2*, 5320–5327.
- (16) Burda, C.; Lou, Y.; Chen, X.; Samia, A. C. S.; Stout, J.; Gole, J. L. *Nano Lett.* **2003**, *3*, 1049–1051.
- (17) Sakhivel, S.; Kisch, H. *ChemPhysChem* **2003**, *4*, 487–490.
- (18) Sakhivel, S.; Janczarek, M.; Kisch, H. *J. Phys. Chem. B* **2004**, *108*, 19384–19387.
- (19) Chen, X.; Lou, Y.; Samia, A. C. S.; Burda, C.; Gole, J. L. *Adv. Funct. Mater.* **2005**, *15*, 41–49.
- (20) Balcerski, W.; Ryu, S. Y.; Hoffmann, M. R. *J. Phys. Chem. C* **2007**, *111*, 15357–15362.
- (21) Reyes-Garcia, E. A.; Sun, Y.; Reyes-Gil, K.; Raftery, D. J. *Phys. Chem. C* **2007**, *111*, 2738–2748.
- (22) Ohno, T.; Mitsui, T.; Matsumura, M. *Chem. Lett.* **2003**, *32*, 364–365.
- (23) Umebayashi, T.; Yamaki, T.; Itoh, H.; Asai, K. *Appl. Phys. Lett.* **2002**, *81*, 454–456.
- (24) Ohno, T.; Tsubota, T.; Toyofuku, M.; Inaba, R. *Catal. Lett.* **2004**, *98*, 255–258.
- (25) Ho, W.; Yu, J. C.; Lee, S. *J. Solid State Chem.* **2006**, *179*, 1171–1176.
- (26) Lettmann, C.; Hildenbrand, K.; Kisch, H.; Macyk, W.; Maier, W. F. *Appl. Catal., B* **2001**, *32*, 215–227.
- (27) Sakhivel, S.; Kisch, H. *Angew. Chem., Int. Ed.* **2003**, *42*, 4908–4911.
- (28) Irie, H.; Watanabe, Y.; Hashimoto, K. *Chem. Lett.* **2003**, *32*, 772–773.
- (29) Choi, Y.; Umebayashi, T.; Yoshikawa, M. *J. Mater. Sci.* **2004**, *39*, 1837–1839.
- (30) Ohno, T.; Tsubota, T.; Nishijima, K.; Miyamoto, Z. *Chem. Lett.* **2004**, *33*, 750–751.
- (31) Rincon, M. E.; Trujillo-Camacho, M. E.; Cuentas-Gallegos, A. K. *Catal. Today* **2005**, *107–108*, 606–611.
- (32) Liu, H.; Imanishi, A.; Nakato, Y. *J. Phys. Chem. C* **2007**, *111*, 8603–8610.
- (33) Dong, C. X.; Xian, A. P.; Han, E. H.; Shang, J. K. *Diffus. Defect Data, Pt. B* **2007**, *121–123*, 939–942.

believed to be involved with the observed increased visible light activity.<sup>39,41,44,45</sup>

Among the most promising materials is carbon-doped TiO<sub>2</sub>,<sup>24,26–33,46–52</sup> hereafter called C-TiO<sub>2</sub>. It has been prepared in several ways. Khan et al. reported that flame pyrolysis of Ti metal with natural gas produced a dark gray material.<sup>50</sup> The color was attributed to (presumably graphitic) carbon impurities remaining in the material. Simple sol–gel techniques have also been used to produce C-TiO<sub>2</sub> using a wide variety of carbon sources, including the titanium alkoxide precursor itself.<sup>26,53–58</sup>

Characterization of the resulting carbon dopant obviously becomes very important, particularly given the divergent synthetic methods. Both coke<sup>26</sup> and carbonate-type species<sup>54,56–59</sup> have been reported. It was also found that oxidation of TiC to C-TiO<sub>2</sub> yields materials in which reduced carbon species remain from some of the Ti–C bonds being preserved through incomplete oxidation.<sup>29,32,60</sup>

In coming to these conclusions, groups report the results of surface-sensitive techniques, such as X-ray photoelectron spectroscopy (XPS), energy-dispersive X-ray spectroscopy

(EDX), or IR spectroscopy. XPS can be particularly useful, in that oxidation states can be immediately determined, but it is not without shortcomings. While XPS gives a good indication of the higher oxidation states of the carbon dopant, signals from adsorbed ambient carbonaceous materials interfere with those of more reduced oxidation states, making identification and quantification of coke difficult. Argon etching can be used to remove adventitious carbon but often results in destroying or completely removing the very surface species that may be crucial to the visible photoactivity of the material.<sup>20</sup> The concentration of carbon can instead be determined by EDX, but this technique also suffers from the exposure to ambient carbon.

We report here a study of C-TiO<sub>2</sub> prepared from <sup>13</sup>C-labeled glucose following the precedent of Xu et al.<sup>56</sup> Labeling with <sup>13</sup>C allows the structural tool of solid state NMR to be added to the array of characterization tools to determine the chemical nature of the dopant. We are also able to show that part of the glucose is covalently bound, with extensive rearrangement, to the TiO<sub>2</sub> during the low-temperature aging process and that the catalyst remains chemically effective.

An analogous study has been carried out with several <sup>15</sup>N-labeled nitrogen precursors in N-TiO<sub>2</sub>.<sup>21</sup> Reyes-Garcia et al. were able to observe probable amino, ammonium, nitrate, and imido species. We expand on the techniques used by these authors, allowing us to remark upon the functionality, quantity, and location of carbon within the samples. The photocatalytic ability of the carbon-modified TiO<sub>2</sub> samples is also reported, using quinoline as an organic probe molecule.

## Experimental Section

Detailed descriptions of the synthetic and analytic methods, along with the degradations, are given in the Supporting Information.

**Preparation of Photocatalysts.** The preparation is based on the procedure reported by Xu et al.<sup>56</sup> Briefly, a 20 mM solution of glucose in ethanol was chilled to near 0 °C and combined with TiCl<sub>4</sub> up to a final Ti concentration of 0.1 M. Aqueous NaOH was added to bring the pH to 5.5, and a yellow gel was obtained after standing for ~150 h. This was dried at 70 °C for 12 h and reground.

In that one purpose of our investigation was to understand the chemical fate of the glucose throughout the process, after grinding, samples were treated in different ways. In some cases (to both remove water-soluble salts and any glucose-derived material not covalently bound to the TiO<sub>2</sub>), the ground samples were thoroughly washed with water before annealing. This step was not part of the Xu protocol.<sup>56</sup> The annealing was conducted under air at 500 °C for 5 min, 120 min, or not at all.

To keep track of these varying materials, a notation is required. The nomenclature used hereafter for the materials follows the format (C)-TiO<sub>2</sub>-(prewashed or not)(calcination time, in minutes), as shown in Table 1. “C” represents the presence of carbon and the type of glucose precursor: C is used when the glucose isotopes were at natural abundance, <sup>13</sup>C<sub>6</sub> is for uniformly labeled glucose, and <sup>13</sup>C1 is for the <sup>13</sup>C label only at carbon 1. The number after TiO<sub>2</sub> indicates the duration of the annealing time, in minutes. A “W” is added before the calcination number if the sample was washed before annealing.

**Routine Physical Characterization.** Physical characterization was carried out using powder X-ray diffraction (XRD), X-ray

- 
- (34) Irie, H.; Watanabe, Y.; Hashimoto, K. *J. Phys. Chem. B* **2003**, *107*, 5483–5486.
- (35) Okato, T.; Sakano, T.; Obara, M. *Phys. Rev. B* **2005**, *72*, 115124/1–115124/6.
- (36) Yang, K.; Dai, Y.; Huang, B. *J. Phys. Chem. C* **2007**, *111*, 12086–12090.
- (37) Liu, S.; Chen, X. *J. Hazard. Mater.* **2008**, *152*, 48–55.
- (38) Asahi, R.; Morikawa, T.; Ohwaki, T.; Aoki, K.; Taga, Y. *Science* **2001**, *293*, 269–271.
- (39) Asahi, R.; Morikawa, T. *Chem. Phys.* **2007**, *339*, 57–63.
- (40) Batzill, M.; Morales, E. H.; Diebold, U. *Phys. Rev. Lett.* **2006**, *96*, 026103/1–026103/4.
- (41) Batzill, M.; Morales, E. H.; Diebold, U. *Chem. Phys.* **2007**, *339*, 36–43.
- (42) Di Valentin, C.; Pacchioni, G.; Selloni, A. *Chem. Mater.* **2005**, *17*, 6656–6665.
- (43) Di Valentin, C.; Finazzi, E.; Pacchioni, G.; Selloni, A.; Livraghi, S.; Paganini, M. C.; Giamello, E. *Chem. Phys.* **2007**, *339*, 44–56.
- (44) Kuznetsov, V. N.; Serpone, N. *J. Phys. Chem. B* **2006**, *110*, 25203–25209.
- (45) Serpone, N. *J. Phys. Chem. B* **2006**, *110*, 24287–24293.
- (46) Wang, H.; Lewis, J. P. *J. Phys.: Condens. Matter* **2005**, *17*, L209–L213.
- (47) Ren, W.; Ai, Z.; Jia, F.; Zhang, L.; Fan, X.; Zou, Z. *Appl. Catal., B* **2007**, *69*, 138–144.
- (48) Wang, X.; Meng, S.; Zhang, X.; Wang, H.; Zhong, W.; Du, Q. *Chem. Phys. Lett.* **2007**, *444*, 292–296.
- (49) Li, Y.; Hwang, D.-S.; Lee, N. H.; Kim, S.-J. *Chem. Phys. Lett.* **2005**, *404*, 25–29.
- (50) Khan, S. U. M.; Al-Shahry, M.; Ingler, W. B., Jr. *Science* **2002**, *297*, 2243–2245.
- (51) Wong, M.-S.; Hsu, S.-W.; Rao, K. K.; Kumar, C. P. *J. Mol. Catal. A* **2008**, *279*, 20–26.
- (52) Cui, X.; Gu, H.; Lu, J.; Shen, J.; Zhang, Z. *J. Nanosci. Nanotechnol.* **2007**, *7*, 3140–3145.
- (53) Sakthivel, S.; Neppolian, B.; Shankar, M. V.; Arabindoo, B.; Palani-chamy, M.; Murugesan, V. *Sol. Energy Mater. Sol. Cells* **2003**, *77*, 65–82.
- (54) Ohno, T.; Tsubota, T.; Nishijima, K.; Miyamoto, Z. *Chem. Lett.* **2004**, *33*, 750–751.
- (55) Xu, C.; Killmeyer, R.; Gray, M. L.; Khan, S. U. M. *Electrochem. Commun.* **2006**, *8*, 1650–1654.
- (56) Xu, C.; Killmeyer, R.; Gray, M. L.; Khan, S. U. M. *Appl. Catal., B* **2006**, *64*, 312–317.
- (57) Xu, T.-h.; Song, C.-l.; Liu, Y.; Han, G.-r. *J. Zhejiang Univ., Sci., B* **2006**, *7*, 299–303.
- (58) Xu, C.; Shaban, Y. A.; Ingler, W. B.; Khan, S. U. M. *Sol. Energy Mater. Sol. Cells* **2007**, *91*, 938–943.
- (59) Xu, C.; Khan, S. U. M. *Electrochem. Solid-State Lett.* **2007**, *10*, B56–B59.
- (60) Irie, H.; Watanabe, Y.; Hashimoto, K. *Chem. Lett.* **2003**, *32*, 772–773.

**Table 1. Description of Preparation and Nomenclature for Synthesized Photocatalysts**

photocatalyst	synthesis description
undoped TiO <sub>2</sub>	prepared without carbon source; annealing time of 5 min
C-TiO <sub>2</sub> -5	prepared with glucose as carbon source; annealing time of 5 min
<sup>13</sup> C <sub>6</sub> -TiO <sub>2</sub> -0	prepared with uniformly <sup>13</sup> C labeled glucose; not annealed
<sup>13</sup> C <sub>6</sub> -TiO <sub>2</sub> -5	prepared with uniformly <sup>13</sup> C labeled glucose; annealing time of 5 min
<sup>13</sup> C1-TiO <sub>2</sub> -0	prepared with glucose containing <sup>13</sup> C label at carbon 1; not annealed
<sup>13</sup> C <sub>6</sub> -TiO <sub>2</sub> -W0	prepared with uniformly <sup>13</sup> C labeled glucose; washed after oven drying; not annealed
<sup>13</sup> C1-TiO <sub>2</sub> -5	prepared with glucose containing <sup>13</sup> C label at carbon 1; annealing time of 5 min
C-TiO <sub>2</sub> -W5	prepared with glucose as carbon source; washed between oven drying and annealing; annealing time of 5 min
<sup>13</sup> C <sub>6</sub> -TiO <sub>2</sub> -W5	prepared with uniformly <sup>13</sup> C labeled glucose; washed between oven drying and annealing; annealing time of 5 min
<sup>13</sup> C1-TiO <sub>2</sub> -W5	prepared with glucose containing <sup>13</sup> C label at carbon 1; washed between oven drying and annealing; annealing time of 5 min
C-TiO <sub>2</sub> -120	prepared with glucose as carbon source; annealing time of 120 min

photoelectron spectroscopy (XPS), and transmission electron microscopy (TEM). Surface area analysis of the materials was performed by nitrogen sorption isotherms in a sorptometer. The surface areas were calculated by the Brunauer–Emmett–Teller (BET) method.

**NMR Parameters.** The NMR experiments were performed on a Bruker DSX400 spectrometer at 400 MHz for <sup>1</sup>H and 100 MHz for <sup>13</sup>C. A Bruker 4-mm triple-resonance magic-angle spinning (MAS) probe head was used for measurements at various MAS speeds. <sup>13</sup>C and <sup>1</sup>H chemical shifts were referenced to TMS, using the COO resonance of α-glycine at 176.49 ppm as a secondary <sup>13</sup>C reference and the proton resonance of NIST hydroxyapatite at 0.18 ppm as a secondary <sup>1</sup>H reference. The 90° pulse lengths were 4 μs for both <sup>13</sup>C and <sup>1</sup>H.

**High-Speed Quantitative <sup>13</sup>C DP/Echo/MAS NMR.** To quantitatively account for the glucose carbon in TiO<sub>2</sub> particles, quantitative direct polarization (DP)/MAS <sup>13</sup>C NMR spectra were acquired at 14 kHz MAS. A Hahn echo was used to avoid baseline distortions and two-pulse phase modulation (TPPM) decoupling was applied during detection. The recycle delays were estimated by measuring cross-polarization (CP)/T<sub>1</sub>/TOSS (total suppression of sidebands) spectra with two or three different T<sub>1,C</sub> filter times. The T<sub>1,C</sub> filter time where the remaining carbon signals were less than 5% of the full intensity was chosen as the recycle delay of the quantitative DP/MAS experiment to ensure that all carbons are essentially fully relaxed. More details are given in ref 61. The recycle delays ranged between 6 and 25 s for the uniformly <sup>13</sup>C-labeled materials and were 100 s for the samples made from singly (<sup>13</sup>C1-)labeled glucose. The measuring time per spectrum was typically 1.5 h. Corresponding quantitative <sup>13</sup>C NMR spectra of nonprotonated carbons and of mobile segments were obtained after recoupled dipolar dephasing of 68 μs duration.

**<sup>13</sup>C Chemical-Shift-Anisotropy Filter.** The <sup>13</sup>C chemical-shift-anisotropy (CSA) filter technique<sup>62,63</sup> with five pulses was used to select signals of sp<sup>3</sup>-hybridized (alkyl) carbons, which have small CSAs due to their nearly tetrahedral bonding symmetry. A filter time of 38 μs and a spinning frequency of 5 kHz were used. For

samples that had not been annealed, cross polarization was used to generate the signal, while direct polarization was used for annealed samples. During detection, TPPM decoupling was applied.

**CH Spectral Editing.** The signals of methine (CH) carbons can be selectively observed based on the CH-group multiple-quantum coherence not being dephased by the spin-pair CH dipolar coupling, while CH<sub>2</sub> group coherence is dephased by the dipolar coupling of the carbon to the second proton.<sup>64</sup> The residual quaternary carbon and partial CH<sub>3</sub> carbon signals were subtracted out by acquiring a second spectrum under the same conditions with an additional 40 μs gated decoupling before detection. The spinning frequency was 5.787 kHz, and the recycle delay was 1.5 s.

**CH<sub>2</sub> Spectral Editing.** Spectral editing of CH<sub>2</sub> signals was achieved by selection of the three-spin coherence of CH<sub>2</sub> groups, using a <sup>13</sup>C 90° pulse and <sup>1</sup>H 0°/180° pulses applied after the first quarter of one rotation period with MREV-8 decoupling.<sup>65</sup> The spinning frequency was 5.787 kHz.

**Two-Dimensional <sup>13</sup>C–<sup>13</sup>C Spin Exchange.** To see the C–C connectivities in the C<sub>6</sub>-TiO<sub>2</sub>-0 sample, a mixing time of 50 ms was used to produce the dipolar <sup>13</sup>C–<sup>13</sup>C spin exchange. For sideband suppression, TOSS was applied before and time-reversed TOSS after the evolution time,<sup>66,67</sup> and normal TOSS was used before detection. Direct polarization with an 8-s recycle delay was used, at a MAS frequency of 7 kHz. The total measurement time was 10 h.

**Selection of Signals of Isolated <sup>13</sup>C Spins.** To determine if the <sup>13</sup>C giving rise to a specific resonance is bonded to another <sup>13</sup>C, dephasing by the homonuclear J-coupling was measured. The dephased signal S after 10 ms of evolution under the J-coupling shows only the signals from isolated <sup>13</sup>C spins. A reference signal S<sub>0</sub> of all spin pairs and isolated <sup>13</sup>C spins was generated by a Hahn-solid-Hahn echo<sup>68</sup> that refocuses the J-coupling.<sup>69</sup> Direct polarization (DP) at a MAS frequency of 14 kHz was used to obtain clear signals from all carbons.

**<sup>13</sup>C{<sup>1</sup>H} HARSHIP NMR.** Heteronuclear Recoupling with Dephasing by Strong Homonuclear Interactions of Protons (HARSHIP)<sup>70</sup> NMR experiments were performed to estimate the distance of the orthocarbonate carbons from the nearest <sup>1</sup>H spins, presumably at the surface of the TiO<sub>2</sub> particles. The spinning frequency was 6.5 kHz.

**<sup>13</sup>C T<sub>1</sub> Relaxation Measurements.** The <sup>13</sup>C T<sub>1</sub> relaxation behavior was measured by DP/T<sub>1</sub>/TOSS with a 20-s recycle delay.<sup>71</sup> The T<sub>1</sub>-filter times varied from 0 to 20 s.

**Degradations.** Suspensions containing 150 μM quinoline and the catalyst (1.0 g/L) were prepared, thoroughly stirred, and saturated with O<sub>2</sub> before photolysis. Reactions were irradiated using the output of broad range 4 W fluorescent tubes centered at 350 nm or light from a 75 W Xe arc lamp passed through a water filter and a 495 nm long pass filter. Small aliquots were removed at appropriate times for kinetics runs, and the concentrations of the partial degradation products were determined by HPLC after removal of the TiO<sub>2</sub>.

(61) Mao, J. D.; Hu, W. G.; Schmidt-Rohr, K.; Davies, G.; Ghabbour, E. A.; Xing, B. *Soil Sci. Soc. Am. J.* **2000**, *64*, 873–884.

(62) Mao, J. D.; Schmidt-Rohr, K. *Solid State Nucl. Magn. Reson.* **2004**, *26*, 36–45.

(63) Chan, J. C. C.; Tycko, R. *J. Chem. Phys.* **2003**, *118*, 8378–8389.

(64) Mao, J. D.; Schmidt-Rohr, K. *J. Magn. Reson.* **2003**, *162*, 217–227.

(65) Mao, J. D.; Schmidt-Rohr, K. *J. Magn. Reson.* **2005**, *176*, 1–6.

(66) Kolbert, A. C.; Griffin, R. G. *J. Magn. Reson.* **1990**, *66*, 87–91.

(67) Geen, H.; Bodenhausen, G. *J. Chem. Phys.* **1992**, *97*, 2928–2937.

(68) Schmidt-Rohr, K.; Spiess, H. W. *Macromolecules* **1991**, *24*, 5288–5293.

(69) Fang, X.-W.; Schmidt-Rohr, K. Manuscript in preparation, 2008.

(70) Schmidt-Rohr, K.; Rawal, A.; Fang, X. W. *J. Chem. Phys.* **2007**, *126*, 054701/1–054701/16.

(71) Torchia, D. A. *J. Magn. Reson.* **1978**, *30*, 613–616.

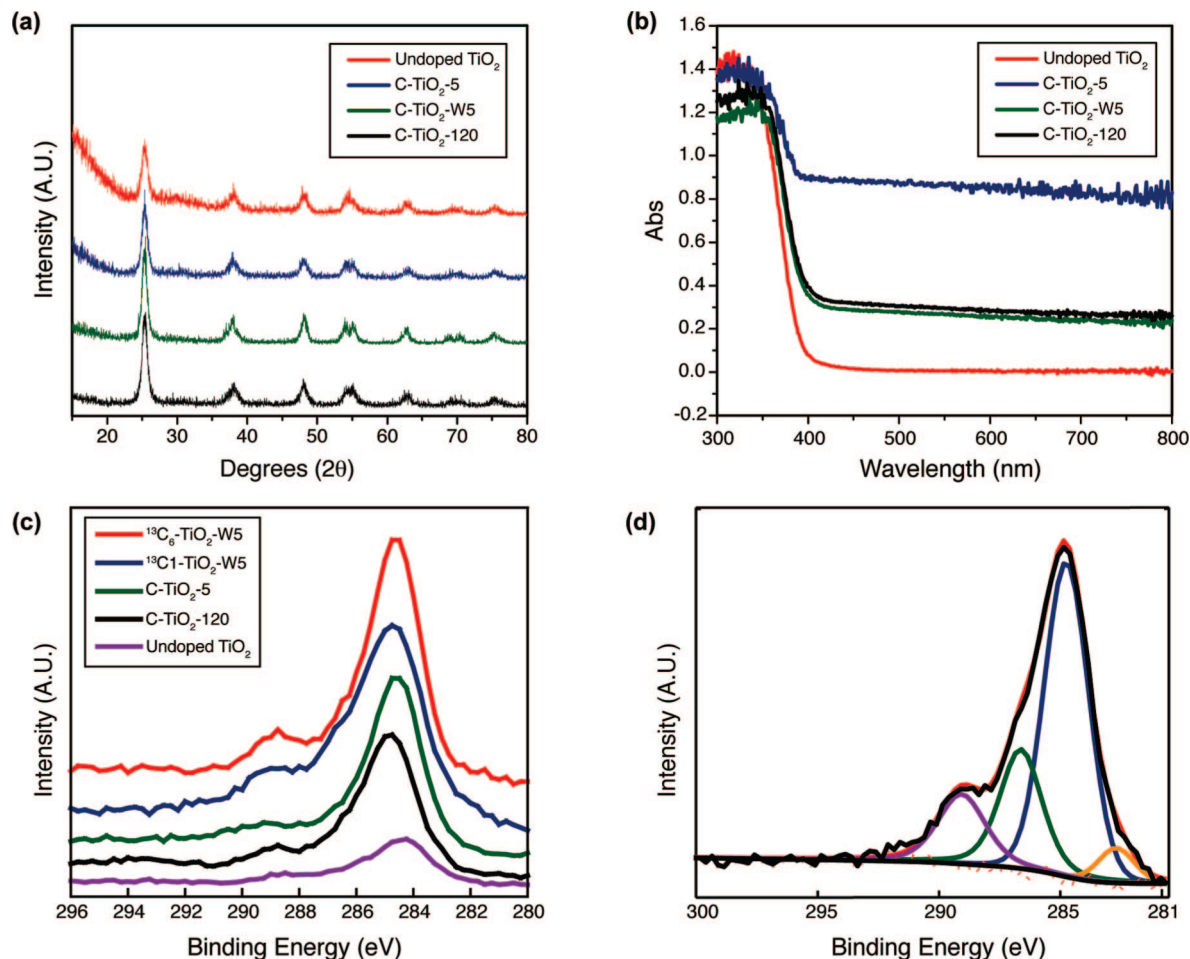


**Figure 1.** (a) X-ray powder diffraction patterns, (b) diffuse reflectance spectra, and (c) XPS spectra of undoped and doped titania. (d) Fitted XP spectrum of <sup>13</sup>C<sub>1</sub>-TiO<sub>2</sub>-W5. Maxima are at 282.4 eV, 284.7 eV, 286.5 eV, and 288.9 eV. See text for discussion.

## Results and Discussion

**Catalyst Preparation.** The preparation of C-TiO<sub>2</sub> by Xu et al.<sup>56</sup> presented a chemically sensible means by which carbon could be covalently attached to the developing TiO<sub>2</sub> framework and was adopted as a model. In most respects, the reported method was used in preparing the current carbon-doped catalysts from glucose and TiCl<sub>4</sub>.<sup>56</sup> An aging time of 150 h was used, following Xu's report of greatest visible light activity. The material obtained after centrifuging the sol-gel was oven-dried at 70 °C for about 12 h.

Characterization of the carbon component by NMR at various stages of the synthesis was a consideration, so after the drying stage, different treatment sequences were undertaken, as shown in Table 1. The variables were whether the dried sample was washed with water before annealing (to remove NaCl and water-soluble glucose-derived components present only as a physical mixture in the TiO<sub>2</sub>) and the length of time of annealing at 500 °C under air. Annealing times were 0, 5, or 120 min, as noted.<sup>72</sup> All carbon-modified materials annealed for 5 min without the additional washing step were dark gray in color. The other annealed samples were an obviously lighter shade of gray.

**Characterization of Annealed Samples by XRD, TEM, XPS, and UV/Vis.** Four classes of samples, including the undoped control material TiO<sub>2</sub>-5, were thoroughly characterized by the classic methods used for these photocatalytic materials, as shown in Figures 1 and 2. The material prepared under conditions most similar to Xu was C-TiO<sub>2</sub>-5. C-TiO<sub>2</sub>-120 was used to determine whether C-TiO<sub>2</sub>-5 would undergo further changes if held at the annealing temperature of 500 °C for a longer time, and C-TiO<sub>2</sub>-W5 was used to help determine whether all of the dopant material was covalently bound to the TiO<sub>2</sub> matrix before the annealing step.

Analysis of all four samples by XRD (Figure 1a) showed them all to be anatase, with average particle diameters of 9–10 nm, as determined by Scherrer's formula ( $d = 0.9\lambda / \beta_{1/2} \cos \theta$ ). TEM images (Figure 2) showed particles with sizes ranging from 5–15 nm, in good agreement. Surface areas, determined by the BET method of N<sub>2</sub> sorption, were also similar, for example, 100 m<sup>2</sup>/g for C-TiO<sub>2</sub>-5, 110 m<sup>2</sup>/g for C-TiO<sub>2</sub>-5, and 114 m<sup>2</sup>/g for C-TiO<sub>2</sub>-120.

Diffuse reflectance UV/vis spectra (Figure 1b) showed the typical onset of absorption near 380 nm for TiO<sub>2</sub>-5, that is, the undoped TiO<sub>2</sub>. Only a subtle red-shift in this absorption is observed in the doped samples. A dramatic increase in nonspecific absorption throughout the visible was observed for C-TiO<sub>2</sub>-5, consistent with its gray color. Di Valentin has suggested that carbon substituting for Ti (see below) does

(72) The Xu protocol called for a 5 min of annealing time.

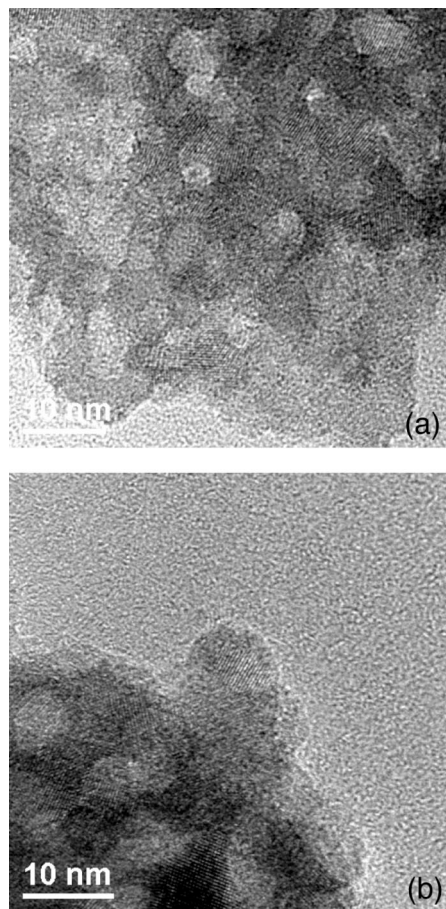


**Figure 2.** TEM images of (a) <sup>13</sup>C<sub>1</sub>-TiO<sub>2</sub>-W5 and (b) <sup>13</sup>C<sub>6</sub>-TiO<sub>2</sub>-5 on the same scale.

not significantly alter the band structure of the TiO<sub>2</sub>, potentially resulting in materials with little visible-light activity.<sup>42</sup> Evidence for several other carbon-containing functional group structures, including coke, which is probably responsible for the nonspecific visible absorption, is presented below.

XPS was used initially to address the character of the carbon dopant in C-TiO<sub>2</sub>-5, the “baseline” doped catalyst, and look for other impurities. Both sodium and chloride were detected in C-TiO<sub>2</sub>-5, presumably due to the presence of these ions in the sol-gel reaction mixture. Multiple types of carbon centers were observed. There are three major components in the C 1s region with binding energies of 288.9 eV, 286.5 eV, and 284.7 eV (Figure 1c). The first two are assigned to carbonate esters and other carbonyls, respectively, based on known chemical shifts.<sup>73</sup> The 284.7 eV peak is attributable to other reduced carbons (C-C/C-H), which can be coke and/or ambient atmospheric species deposited on the surface. Fitting the data to Gauss-Lorentz curves (70–95% Gauss) reveals a small shoulder at 282.4 eV, possibly arising from a Ti-C bond. This phenomenon is illustrated using the spectrum of C-TiO<sub>2</sub>-W5 in Figure 1d. Argon etching and remeasurement generally resulted in significant reduction of the peaks attributed to oxidized carbon species, leaving mostly C-C/C-H species and the shoulder at 282.4 eV. The signal at 282.4 eV often became more prevalent after argon etching. Since the materials are annealed under oxidative conditions, it is more likely that

this Ti-C species suggested by the 282.4 eV peak is present as an interstitial carbon also bound to oxygen, as opposed to a highly reduced carbon substituting for oxygen.<sup>42,74</sup>

Annealing the sample for 2 h, rather than 5 min (i.e., C-TiO<sub>2</sub>-120), resulted in a material that was visibly lighter in color, and this is reflected quantitatively in the UV/vis spectrum (Figure 1b), but the XPS data were essentially unchanged from C-TiO<sub>2</sub>-5.

Insertion of a washing step before annealing (C-TiO<sub>2</sub>-W5), as expected, resulted in a material in which no sodium or chloride was detected by XPS. The carbon portion of the XPS spectrum was essentially unchanged. However, the C-TiO<sub>2</sub>-W5 was a lighter color, quite similar to that of C-TiO<sub>2</sub>-120, as reflected in the UV/vis data. This suggested that there was less organic material and pointed out some of the difficulty of quantifying the carbon by XPS.

XPS data were also collected for the undoped TiO<sub>2</sub>-5 as a control. Neither sodium nor chloride was detected. However, a smaller but easily detectable amount carbon was seen, with weaker signals at 288.9 eV, 286.5 eV, and 284.7 eV.<sup>75</sup> Importantly, however, no carbon remained detectable after argon etching of thoroughly washed TiO<sub>2</sub>-5. This implies that the carbon signals were due to adventitious adsorbed carbon, as alluded to in the Introduction.

**NMR Analysis.** The controls in the XPS data suggest that the those spectra indeed do reflect “ambient” carbon when obtained under ordinary aerobic conditions. NMR data were obtained for analogous materials prepared with <sup>13</sup>C-labeled glucose to increase sensitivity and allow for measurement of C-C coupling. Also, the NMR data reveal more detail about functional group identity and location.

*Analysis of Preannealed Samples.* <sup>13</sup>C NMR spectra of the samples after glucose is exposed to the titanium-containing precursor but before annealing (<sup>13</sup>C<sub>6</sub>-TiO<sub>2</sub>-0) are shown in Figures 3 and 4. The reaction causes significant changes to glucose, as seen by the comparison to a reference spectrum in Figure 3a. The quantitative spectrum of Figure 3b exhibits many new bands, spanning much of the spectral range of <sup>13</sup>C. They can be assigned on the basis of their chemical shifts and CH<sub>n</sub> spectral editing, as shown in Figure 3b–e. The strongest signal, at ~83 ppm, with a shoulder at ~73 ppm, is due to OCH methine groups (Figure 3d). Several unresolved bands of O-CH-O methine groups are detected between 100 and 115 ppm, but there are no signals of CH groups not bonded to O, which would resonate at ~50 ppm. In the CH<sub>2</sub>-only spectrum of Figure 3e, we observe not only a C-CH<sub>2</sub>-C methylene resonance at 38 ppm and a CH<sub>2</sub>-OH methylene peak at 63 ppm but also a strong OCH<sub>2</sub> methylene band with a maximum at an unusually high frequency chemical shift of ~78 ppm.

(73) Moulder, J. F.; Stickle, W. F.; Sobol, P. E.; Bomben, K. D. *Handbook of X-Ray Photoelectron Spectroscopy*; Perkin-Elmer Corporation (Physical Electronics): Eden Prairie, MN, 1992.

(74) The ordinary chemical shift for TiC is 281.7 eV.

(75) It should be noted that the fits were done using standard Gauss-Lorentz symmetric peaks (70–95% Gauss) for the C 1s region since there was no apparent reason to deviate for normal parameters (Figure 1d). It is possible that certain peaks could be made less significant or absent by changing certain parameter limits.

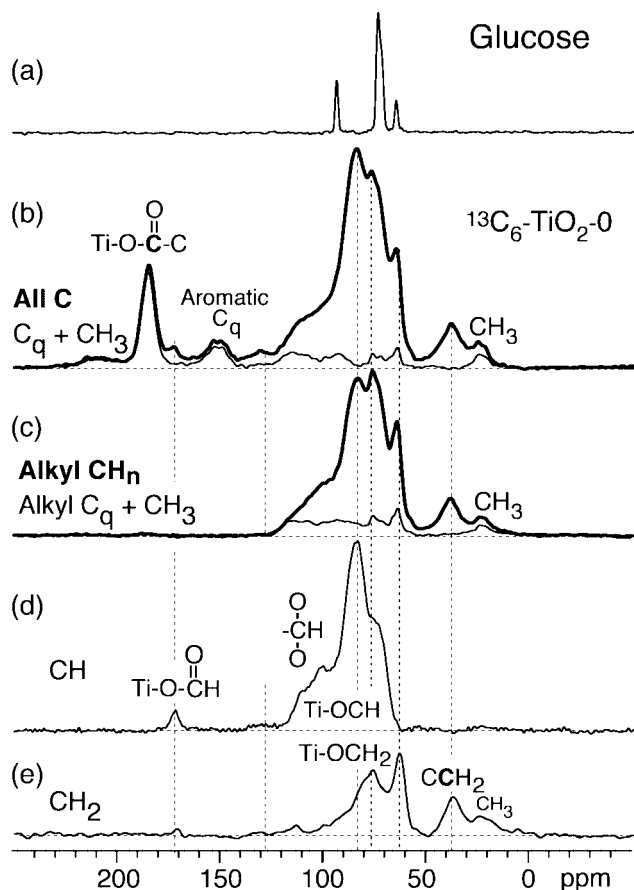


**Figure 3.** <sup>13</sup>C NMR spectra of materials before annealing. (a) Spectrum of glucose for reference. (b–e) Spectra of <sup>13</sup>C<sub>6</sub>-TiO<sub>2</sub>-0 with spectral editing. (b) Quantitative spectrum of all C (thick line) and corresponding spectrum of nonprotonated C plus CH<sub>3</sub> (thin line) at 14 kHz MAS. (c) Spectrum after a chemical shift anisotropy (CSA) filter, which selects signals of sp<sup>3</sup>-hybridized carbons (thick line), with signals extending to 120 ppm. The corresponding spectrum of quaternary carbon and CH<sub>3</sub> signals (thin line) was selected by 40 μs of gated decoupling before detection. (d) CH-only and (e) CH<sub>2</sub>-only spectra. All CH are polar alkyl and substituted by oxygen, according to their high-frequency chemical shift.

A strong COO ester-type signal at 183 ppm, as well as weaker signals of ketones at ~210 ppm, of CH<sub>3</sub> groups at ~22 ppm, and of aromatic C (mostly furan at ~150 ppm), is identified after C–H dipolar dephasing (Figure 3b, thin line).

The resonance frequencies of the strongest OCH methine, O–CH–O methine, OCH<sub>2</sub> methylene, and COO ester-type signals are all at unusually high frequencies, by about 10 ppm, from their usual positions in organic compounds.<sup>76</sup> This is an indication of bonding to Ti via the O, since the literature shows a comparable chemical shift for <sup>13</sup>C in Ti–O–CH<sub>2</sub> groups.<sup>77</sup> After a chemical shift anisotropy filter that selects sp<sup>3</sup> hybridized carbons (Figure 3c), the alkyl signals are seen to extend to 130 ppm, again at unusually high frequency.

The CH-only spectrum (Figures 3d and 4c) also reveals a small signal of an unusual methine resonating at 170 ppm, which is found to be an isolated <sup>13</sup>C (not bonded to other C) in J-dephasing experiments. On that basis, the peak at 170 ppm is assigned to a formate ester R–O–CHO, where the

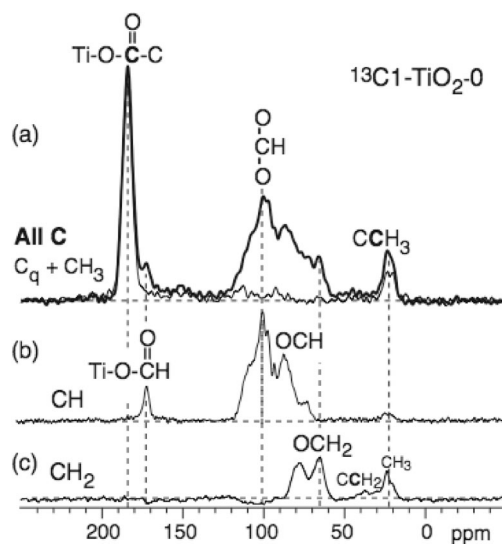


**Figure 4.** <sup>13</sup>C NMR of <sup>13</sup>C<sub>1</sub>-TiO<sub>2</sub>-0 with spectral editing. (a) Quantitative spectrum of all C (thick line) and nonprotonated C (thin line) at 14 kHz MAS. (b) CH-only and (c) CH<sub>2</sub>-only spectra, with residual CH<sub>3</sub> signals near 24 ppm.

unusually high frequency chemical shift from 160–165 ppm for R = C<sup>76</sup> indicates that R = Ti. By control experiments described in the Supporting Information, we have excluded that the simple harshly acidic reaction conditions were responsible for the high-frequency chemical shifts (and the other rearrangements of glucose). We cannot rule out a small amount of direct C–Ti bonding, as hinted at by the XPS data, which might be obscured by other oxygenated functionality.<sup>78</sup>

Further information about the connectivity of the observed carbon species was obtained by selective labeling from glucose–<sup>13</sup>C<sub>1</sub> and by <sup>13</sup>C–<sup>13</sup>C correlations on the fully <sup>13</sup>C-labeled sample. The spectrum of <sup>13</sup>C<sub>1</sub>-TiO<sub>2</sub>-0 (i.e., dried but unannealed material) is dominated by the ester-type COO–Ti signal; comparison with the peak intensity for the fully labeled sample shows that glucose C1 accounts for only about half of this species. This proves that significant rearrangement involving C1 has occurred. In addition, the glucose C1 site contributes to about half of the C–CH<sub>3</sub> species but does not form C–CH<sub>2</sub>–C methylenes and relatively little OCH methine or OCH<sub>2</sub> methylene. A large fraction of the O–CHR–O methine species comes from C1, as in the original structure of glucopyranose.

The <sup>13</sup>C–<sup>13</sup>C correlation spectrum of <sup>13</sup>C<sub>6</sub>-TiO<sub>2</sub>-0 is shown in Figure 5a. It shows pronounced cross peaks between COO (ester-type) and OCH methine, COO and CH<sub>2</sub> (meaning C–CH<sub>2</sub>–C), OCH methine and other OCH methines, OCH methine and OCH<sub>2</sub> methylene, and OCH and CH<sub>2</sub>, as well as OCH and O–CH–O signals. On the basis of these and the <sup>13</sup>C<sub>1</sub> labeling pattern, we propose two likely six-carbon fragments (Figure 5b). They account for the observed cross peaks of both CH<sub>2</sub> (not bonded to O) and Ti–O–CH methine carbons to COO groups, which were shown to be predominantly contributed by C1 of glucose. The CH<sub>2</sub>–CH–O–Ti, OCH–CHO, and OCH–CH<sub>2</sub>–O–Ti connectivities of the model structures are also seen in the spectrum. The cross-peak pattern of furan (150–110 ppm) is also detected. Other structures accounting for the remaining carbon species must

(76) Pretsch, E.; Bühlmann, P.; Affolter, C. *Structure Determination of Organic Compounds: Tables of Spectral Data*, Third Completely Revised and Enlarged English ed.; Springer: New York, 2000.

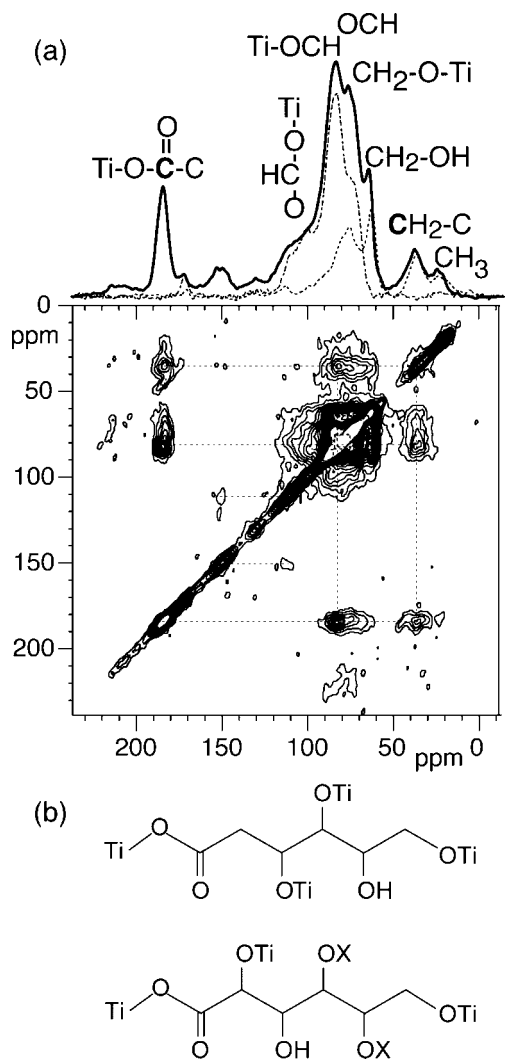


**Figure 5.** (a) Two-dimensional  $^{13}\text{C}$ - $^{13}\text{C}$  correlation spectrum of  $^{13}\text{C}_6$ -TiO<sub>2</sub>-0 with a mixing time of 50 ms at 14 kHz MAS. At the top, one-dimensional spectra of all C (thick line), CH (dash-dotted line), and CH<sub>2</sub> (dashed line) are shown superimposed to facilitate peak assignment. (b) Two structural fragments consistent with the observed cross peaks in (a).

also be present and might be identified in a more detailed study; however, since high-temperature annealing greatly transforms the existing structures, the details of these structures may be of limited relevance for the final forms of carbon in the TiO<sub>2</sub> photocatalyst.

Figure 8 compares  $^{13}\text{C}$  NMR spectra of samples with and without washing with water but without annealing ( $^{13}\text{C}$ -TiO<sub>2</sub>-W0 vs  $^{13}\text{C}$ -TiO<sub>2</sub>-0). Only subtle changes are observed (Figure 8a,b). Washing removes the minor furan-like components and increases the signal for some C=O species, which in effect fill the volume vacated by the components that were washed out. However, after collection and lyophilization of the aqueous washes, little organic material was observed by either  $^1\text{H}$  or  $^{13}\text{C}$  solution-phase NMR, confirming that most of the material removed by the washing step was NaCl.

**NMR of Annealed Samples.** High-temperature annealing dramatically alters the forms of carbon in the samples, mostly leading to dehydration and condensation. The spectra in Figure 6a,b for samples annealed at 500 °C for 5 and 120 min ( $^{13}\text{C}_6$ -TiO<sub>2</sub>-5 and  $^{13}\text{C}_6$ -TiO<sub>2</sub>-120), respectively, are dominated by a broad aromatic-carbon band at 130 ppm. Of

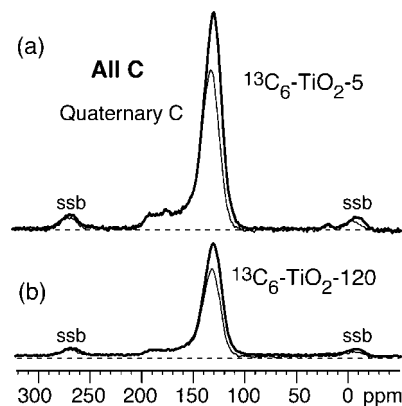


**Figure 6.** Comparison between the quantitative  $^{13}\text{C}$  NMR spectra of (a)  $^{13}\text{C}_6$ -TiO<sub>2</sub>-5 and (b)  $^{13}\text{C}_6$ -TiO<sub>2</sub>-120, plotted on a correct relative vertical scale. Thick lines, spectra of all C; thin lines, spectra of quaternary C. Spinning frequency: 14 kHz. Spinning side bands are marked ssb.

these aromatics,  $72 \pm 2\%$  are not protonated, which suggests fused aromatic rings. (For example, all of the carbons of benzene are protonated, and essentially none of those in a large graphene sheet are protonated.) In addition, a clear shoulder between 170 and 200 ppm, assigned to C=O species, is observed if the sample annealed for only 5 min ( $^{13}\text{C}_6$ -TiO<sub>2</sub>-5), and the total signal intensity is greater.

When the washing step is inserted between drying and annealing ( $^{13}\text{C}$ -TiO<sub>2</sub>-W5), an interesting and reproducible spectral feature is observed that is not found using any of the other protocols: a sharp peak at 126 ppm (Figure 7). This peak integrates to 37% of the total intensity, and it is also noted that the carbonate ester peak (Figure 8) is more pronounced. While the chemical shift of 126 ppm might initially suggest an aromatic carbon, spectral editing proves that it must be assigned to a tetracoordinate alkyl orthocarbonate (C(OR)<sub>4</sub>) functionality. Gated decoupling proves that this is a nonprotonated carbon (Figure 7a). It experiences no J-coupling to another  $^{13}\text{C}$ , as proved by the absence of J-dephasing (Figure 7b); thus, it cannot be bonded to  $^{13}\text{C}$ , which rules out an aromatic structure. This is confirmed by the minimal dephasing by a CSA-filter, which is characteristic of an sp<sup>3</sup>-hybridized carbon with nearly tetrahedral bonding symmetry.<sup>62</sup>

Given that the four bonds cannot be to carbon or hydrogen, orthocarbonate is the only reasonable structure. Such a structure is in good agreement with the observed unusually high field chemical shift: ketals and acetals resonate around 100 ppm, orthoesters resonate at approximately 115 ppm, and orthocarbonate bands generally arise around 120 ppm.<sup>76</sup> To the best of our knowledge, no previous reports of an orthocarbonate center in TiO<sub>2</sub> have been made. The narrow line shape (Figure 7c) is indicative of a well-defined crystalline environment, strongly suggesting that the orthocarbonate centers are incorporated into the TiO<sub>2</sub> lattice. Direct substitution of C for Ti, which would result in hexacoordinate carbon, seems unlikely given the DFT calculations of Di Valentin et al.<sup>42</sup> which did not yield any low-energy structure with six-coordinate C for anatase or rutile. Instead, substitution of C for Ti (“C<sub>8</sub>-Ti”) in anatase has been predicted to result in a low-energy structure with C in a tetrahedral bonding environment.<sup>42</sup>

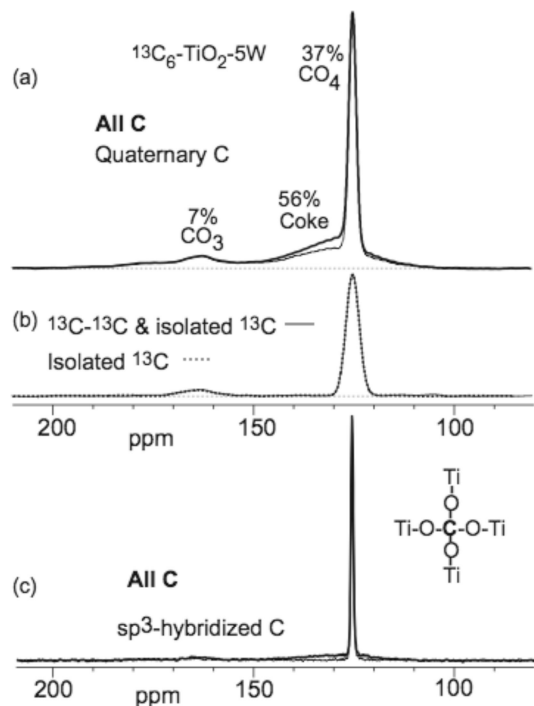


**Figure 7.**  $^{13}\text{C}$  NMR spectra of  $^{13}\text{C}_6\text{-TiO}_2\text{-W5}$ . (a) Quantitative (DP) spectrum of all C (thick line) and corresponding spectrum of nonprotonated C (thin line). Strong line broadening was applied to make the coke and  $\text{CO}_3$  bands more visible. (b) J-modulated dephasing spectra. Solid line: Reference spectrum  $S_0$  of  $^{13}\text{C}$ – $^{13}\text{C}$  spin pairs and isolated  $^{13}\text{C}$  spins. Dashed line: Spectrum S after dephasing by  $^{13}\text{C}$ – $^{13}\text{C}$  J-coupling. The two spectra are very similar and prove that the two sharp peaks are from isolated carbons. Strong line broadening was applied to make the  $\text{CO}_3$  band more visible. (c) Selection of  $\text{sp}^3$ -hybridized C by a five-pulse CSA filter. Thick line: reference spectrum with minimum CSA dephasing time (1  $\mu\text{s}$ ). Thin line: spectrum after a CSA dephasing time of 38  $\mu\text{s}$  at 6.5 kHz MAS. In this spectrum with minimal line broadening applied, the small natural width of the peak at 126 ppm is apparent.

A distinct  $^{13}\text{C}$  signal is also observed around 163 ppm. Lack of C–H dipolar and C–C J-dephasing (Figure 7a,b) shows that this carbon also is not protonated and not bonded to another C. However, its signal is suppressed by the CSA filter, proving that this is an  $\text{sp}^2$ -hybridized C. On this basis, we identify this as a  $\text{CO}_3$  (regular carbonate) moiety, which is in good agreement with its chemical shift. According to Di Valentin et al., such a planar  $\text{CO}_3$  unit can be formed by interstitial (“ $\text{C}_1$ ”) carbon in anatase.<sup>42</sup>

The dephasing of the orthocarbonate signal in  $^{13}\text{C}\{^1\text{H}\}$ -HARDSHIP<sup>70</sup> distance measurements is very slow compared to coke in the same sample and still slow relative to that of carbon in 4.8-nm diameter nanodiamond with protonated surfaces, as shown in Figure 9. This indicates that the orthocarbonate species is far (>1 nm) from any  $^1\text{H}$ : it is thus not a surface species, which may be why it is not observed in the XPS spectrum. By contrast, the fast dephasing of the coke signal in Figure 9 demonstrates that the coke component is close to protons, suggesting this species is on the surface containing aromatic C–H and possibly nearby Ti–OH bonds.

Further structural information can be gleaned from the observed spin–lattice relaxation times. Figure 10 shows that the two major components of  $^{13}\text{C}_6\text{-TiO}_2\text{-W5}$  have similarly short  $^{13}\text{C}$  spin lattice relaxation times of near 3 s. These  $T_1$  relaxation values are too short to be produced by the relevant internuclear couplings or chemical shift anisotropies. We

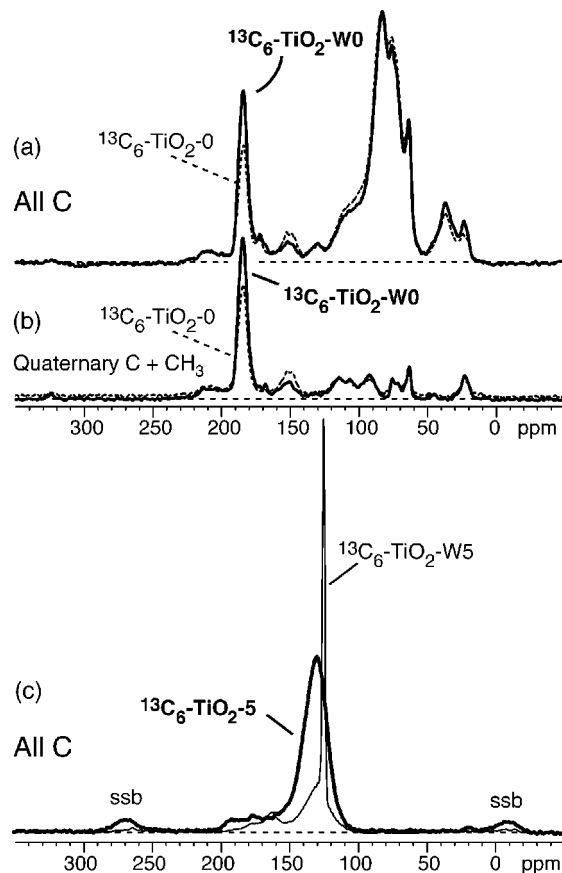


**Figure 8.** Effects of washing oven-dried material before annealing on  $^{13}\text{C}$  spectra before and after annealing. (a) Quantitative  $^{13}\text{C}$  NMR spectra of  $^{13}\text{C}_6\text{-TiO}_2\text{-W0}$  (solid line) and of  $^{13}\text{C}_6\text{-TiO}_2\text{-0}$  (dashed line). (b) Corresponding quantitative spectra of quaternary and methyl C. (c) Quantitative  $^{13}\text{C}$  NMR spectra of  $^{13}\text{C}_6\text{-TiO}_2\text{-W5}$  (thin line) and of  $^{13}\text{C}_6\text{-TiO}_2\text{-5}$  (thick line).

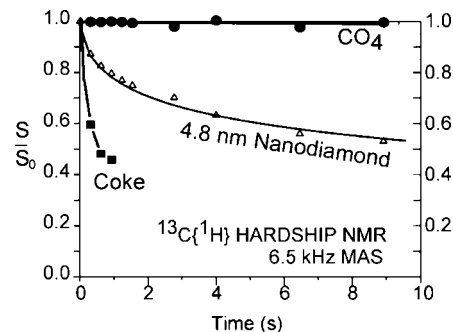


**Figure 9.**  $^{13}\text{C}\{^1\text{H}\}$  HARDSHIP NMR decay curves of the orthocarbonate and coke signals in  $^{13}\text{C}_6\text{-TiO}_2\text{-W5}$ . The decay curve for 4.8-nm diameter nanodiamond is used as a reference. The slow decay of the  $\text{CO}_4$  signals shows that orthocarbonate is located deep inside the  $\text{TiO}_2$  nanoparticles.

conclude that the short  $T_1$  must be attributed to fluctuating fields produced by unpaired electrons; these have been detected by EPR and attributed to electron vacancies by other workers.<sup>49</sup> The nonexponential relaxation is typical of this process, with  $T_1 \sim r_{\text{ce}}^{-6}$ , where  $r_{\text{ce}}$  is the distance between the  $^{13}\text{C}$  and the unpaired electron: faster-decaying components arise from carbons closer to the unpaired electron center, and carbons further from the unpaired electron decay more slowly.

**Carbon Weight Fractions from NMR.** The amount of carbon is an important structural parameter of C-doped  $\text{TiO}_2$ .

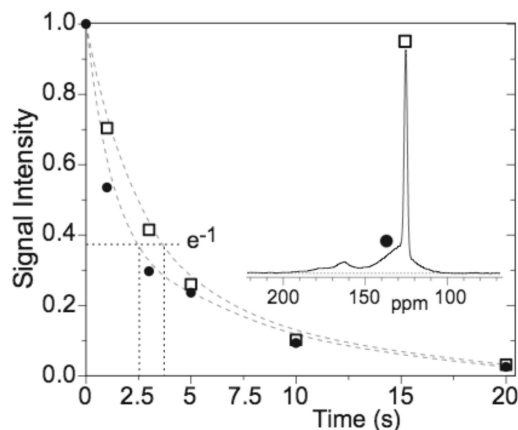


**Figure 10.** <sup>13</sup>C spin–lattice relaxation time measurements of orthocarbonate (CO<sub>4</sub>) centers (squares) and coke (circles) in <sup>13</sup>C<sub>6</sub>-TiO<sub>2</sub>-W5. The dashed lines are guides to the eye. These nonexponential decays have 1/e times of approximately 3.5 and 2.5 s, respectively.

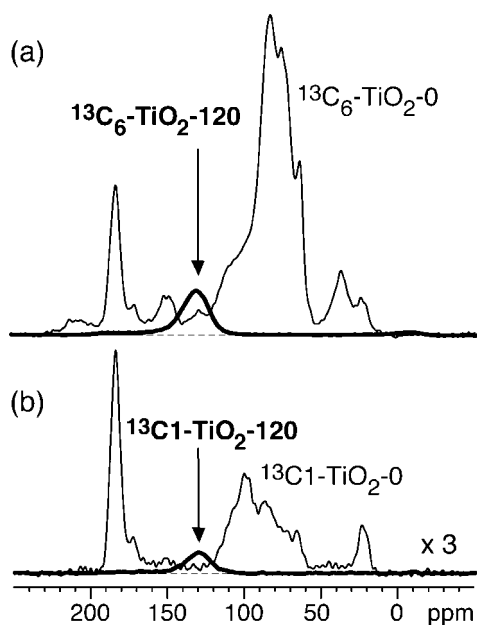


**Figure 11.** Comparison between the quantitative spectra of Ti-containing materials before and after annealing. (a) Comparison of <sup>13</sup>C<sub>6</sub>-TiO<sub>2</sub>-0 (dashed line) and <sup>13</sup>C<sub>1</sub>-TiO<sub>2</sub>-0 (solid line), plotted on a correct relative vertical scale. (b) Comparison of <sup>13</sup>C<sub>1</sub>-TiO<sub>2</sub>-0 (thin line) and <sup>13</sup>C<sub>1</sub>-TiO<sub>2</sub>-120 (thick line). Part b is scaled up by 300% relative to part a.

Traditional combustion analysis may not detect all C incorporated within the TiO<sub>2</sub> lattice; this limitation is not present in carbon quantification by <sup>13</sup>C NMR. Figure 11 compares the <sup>13</sup>C NMR signal intensity for samples before and after annealing, confirming a major loss of carbon. The carbon mass fractions in the six samples studied were determined from the total integrated intensity of the direct-polarization <sup>13</sup>C NMR spectra, normalized per scan and mass of sample in the rotor (Figure 12). On the basis of a calibration line determined by NMR and elemental analysis of several model compounds (circles) and validated on many samples of plant and soil organic matter (open triangles),<sup>79</sup>

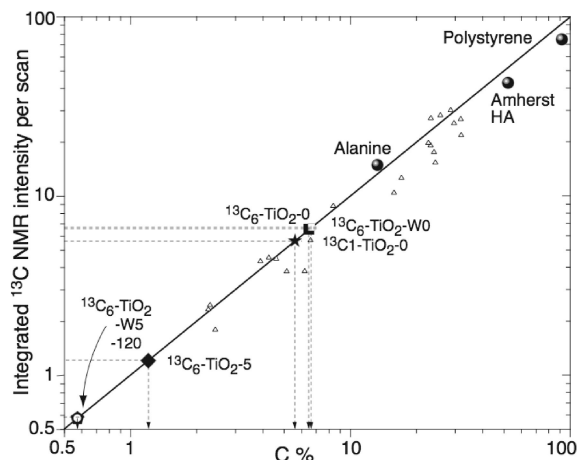


**Figure 12.** Carbon mass percentages in glucose–<sup>13</sup>C modified TiO<sub>2</sub> from correlations of integrated DP <sup>13</sup>C NMR intensities per scan and milligrams of sample (ordinate) with the carbon mass fractions from elemental analysis (abscissa), calibrated using alanine, polystyrene, humic acid from Amherst, and numerous soil samples (open triangles). <sup>13</sup>C<sub>6</sub>-TiO<sub>2</sub>-0, filled square; <sup>13</sup>C<sub>1</sub>-TiO<sub>2</sub>-0, star; <sup>13</sup>C<sub>6</sub>-TiO<sub>2</sub>-W0, open small square; <sup>13</sup>C<sub>6</sub>-TiO<sub>2</sub>-W5, filled diamond; <sup>13</sup>C<sub>6</sub>-TiO<sub>2</sub>-120 filled pentagon; and <sup>13</sup>C<sub>6</sub>-TiO<sub>2</sub>-W5, open pentagon. The degree of <sup>13</sup>C labeling has been taken into account in determining the overall carbon percentage. Carbon content declines substantially on extended annealing.

the measured <sup>13</sup>C NMR intensity of each sample studied here was converted to an approximate carbon weight percent (taking into account the <sup>13</sup>C labeling level). The three samples before annealing have 5.5–6.5 wt % C, which corresponds to an organic volume fraction around 15%, given the ~2.5 times higher density of TiO<sub>2</sub> relative to glucose. Without washing, 5-min annealing reduces the carbon to 1.2 wt % and 120-min annealing further to 0.6 wt %. After washing and 5-min annealing, the carbon weight fraction is also 0.6 wt %.

In summary, the NMR data strongly suggest there is more than a physical interaction between the glucose and the titanium-containing precursor, and chemical reaction does occur during the aging and/or drying stages. Upon annealing of washed samples, carbon trapped inside the TiO<sub>2</sub> particles ultimately ends up substituting for a Ti atom, and carbon nearer to the surface seems to be condensed into coke.

**Photocatalytic Activity.** The purpose of doping TiO<sub>2</sub> is to produce a catalyst with visible absorption that also at least maintains, if not improves on, the oxidative activity. Though NMR characterization of the carbon in C-TiO<sub>2</sub> is the central point of this paper, at least a meaningful screening for photocatalytic activity is essential. Ordinarily, TiO<sub>2</sub> photocatalyzes oxidative reactions either by initiating an oxidative single electron transfer (SET) or by invoking hydroxyl-radical-like reactivity. The dopant has the potential to hinder, as well as enhance, this property. For example, discrete dopant centers interject filled midgap orbitals into the semiconductor band structure, and their visible-light activation may result in much different and potentially less powerful oxidative behavior. Similarly, absorption by a color center such as graphite would set off a different set of microscopic events (e.g., electron injection into the TiO<sub>2</sub>) that could again result in much different oxidative behavior. Thus, a short series of experiments was conducted to

(77) Foris, A. *Magn. Reson. Chem.* **2000**, *38*, 1044–1046.

(78) Berger, S.; Bock, W.; Frenking, G.; Jonas, V.; Müller, F. *J. Am. Chem. Soc.* **1995**, *117*, 3820–3829.

(79) Fang, X.-W.; Chua, T.; Schmidt-Rohr, K.; Thompson, M. L. *Org. Geochem.* **2008**, submitted.

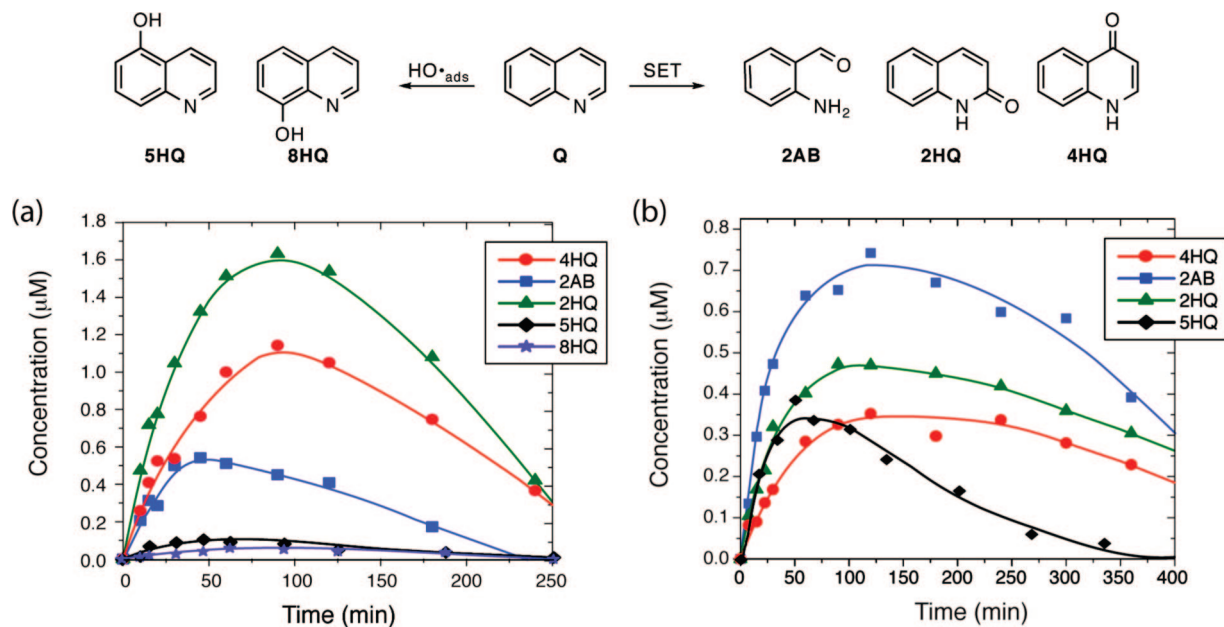


**Figure 13.** Photocatalytic degradation of quinoline: (a) loss of quinoline; formation of 4HQ, 2AB, and 2HQ mediated by (a) undoped  $\text{TiO}_2-0$  and (b)  $\text{C-TiO}_2\text{-W5}$  under 350 nm irradiation.

preliminarily screen the  $\text{C-TiO}_2$  derivatives for their photocatalytic activity.

We chose quinoline as a preliminary probe for  $\text{C-TiO}_2$  reactivity. Methylene blue has commonly been used as a probe for reactivity, but it has significant shortcomings that have been pointed out elsewhere.<sup>80</sup> We have advocated the use of 4-methoxyresorcinol,<sup>81</sup> but it and related molecules can form charge transfer complexes that are inherently subject to visible light photolysis.<sup>82–85</sup> Quinoline does not have these problems. Its chemistry under photocatalytic conditions has been described in detail,<sup>86,87</sup> but the essential results of its earliest degradation steps are that it suffers SET mainly on the pyridine nucleus and hydroxyl attack mainly on the benzene nucleus, as illustrated in Figure 13.

The rates of the initial degradation steps of quinoline were within a factor of 1.5 of one another for  $\text{TiO}_2-5$ ,  $\text{C-TiO}_2\text{-W5}$ , and  $\text{C-TiO}_2-5$  for photolysis at pH 6 using irradiation centered at 350 nm (fwhm  $\sim 50$  nm). Thus, the presence or absence of coke on the surface of  $\text{TiO}_2$  did not have a large effect on the degradation rate. Full data are given in the Supporting Information.

None of the current carbon-doped materials showed significant visible light photoactivity with quinoline upon  $\geq 495$  nm photolysis. These results clearly demonstrate that the presence of graphite on the  $\text{TiO}_2$  surface is *not* the cause

of any detected visible light activity. It is worth stressing that we believe quinoline is a fairly rigorous test of visible light reactivity, as a result of its lack of charge transfer bands and modest adsorption characteristics.

The product distributions obtained with the broad 350 nm-centered irradiation were also examined. Undoped  $\text{TiO}_2-5$  and  $\text{C-TiO}_2-5$  led to similar early product distributions, with the SET-initiated products (functionalizing the pyridine nucleus) being the major pathways. Interestingly,  $\text{C-TiO}_2\text{-W5}$  gave a significantly different product distribution than the other photocatalysts (Figure 13). The most significant difference is that 5HQ was formed as one of the major products, it representing the onset of the hydroxyl radical pathways. Among the SET products, 2HQ was still quite prominent, but 2AB was formed in greater proportion. It is tempting to correlate the product distribution change with the newly characterized orthocarbonate centers, but this must be seen as speculative, particularly since they are not associated with the surface, and their mechanism of action would thus have to be indirect.

## Conclusions

NMR is shown to be a useful tool for probing the structure of magnetically accessible nuclei in carbon-doped  $\text{TiO}_2$ . It shows that a strategy of using glucose (as a representative polyol) as a dopant does provide true covalent interactions ( $\text{Ti-O-C}$  bonds) in the sol-gel stage of the catalyst preparation and, furthermore, that significant chemical change of the carbon structure occurs during this time. It confirms the previously somewhat ambiguous conclusion that coke is the major carbon-containing component of most of these hybrid materials but also shows that orthocarbonate structures, with C-for-Ti substitutions deep inside the titania particles, and regular carbonate moieties do occur in annealed samples when a washing step is inserted between the initial drying and annealing. The removal of small amounts of

(80) Yan, X.; Ohno, T.; Nishijima, K.; Abe, R.; Ohtani, B. *Chem. Phys. Lett.* **2006**, *429*, 606–610.

(81) Hathway, T.; Jenks William, S. *J. Photochem. Photobiol. A* **2008**, in press.

(82) Agrios, A. G.; Gray, K. A.; Weitz, E. *Langmuir* **2003**, *19*, 1402–1409.

(83) Agrios, A. G.; Gray, K. A.; Weitz, E. *Langmuir* **2004**, *20*, 5911–5917.

(84) Kim, S.; Choi, W. *J. Phys. Chem. B* **2005**, *109*, 5143–5149.

(85) Orlov, A.; Watson, D. J.; Williams, F. J.; Tikhov, M.; Lambert, R. M. *Langmuir* **2007**, *23*, 9551–9554.

(86) Cermenati, L.; Pichat, P.; Guillard, C.; Albini, A. *J. Phys. Chem. B* **1997**, *101*, 2650–2658.

(87) Nicolaescu, A. R.; Wiest, O.; Kamat, P. V. *J. Phys. Chem. A* **2005**, *109*, 2829–2835.

furan-like materials by washing does not seem like an adequate rationalization to explain the changes. It is possible that this change is instead a result of the presence of water at the beginning of the annealing period, but this interpretation remains speculative. Carbon doping does not qualitatively affect the rate of photocatalytic degradation of quinoline, or the predominance of SET-induced products in the early stages of degradation at pH 6, except for the C-TiO<sub>2</sub>-W5 catalyst. Here, hydroxyl chemistry was more competitive, just as the orthocarbonate structure was only observed in this material. However, the causality of this association is not established. Inasmuch as visible light irradiation ( $\geq 495$  nm) does not photocatalyze decomposition of quinoline but that a reasonable rationalization for this exists through the intervention of the coke, we suggest that preparing coke-free C-TiO<sub>2</sub> may be critical for proving the

utility of orthocarbonate-containing TiO<sub>2</sub> for visible-light applications.

**Acknowledgment.** The authors thank the National Science Foundation (CHE 0518586) for financial support of this work. We are grateful to Clemens Burda for allowing us to obtain diffuse reflection spectra on his instrumentation. We also gratefully acknowledge the assistance of Jim Anderegg with the XPS data.

**Supporting Information Available:** Additional experimental details and more information about the control experiments on materials before annealing and photocatalytic degradation of quinoline. This material is available free of charge via the Internet at <http://pubs.acs.org>.

CM8019445